Novel two-stage fluidized bed-plasma gasification integrated with SOFC and chemical looping combustion for the high efficiency power generation from MSW: A thermodynamic investigation

Peng Jiang a,b, Ashak Mahmud Parvez c, Yang Meng a, Xinyue Dong a, Mengxia Xu a,d, Xiang Luo a,d, Kaiqi Shi a,d, Tao Wu

University of Nottingham
UK | CHINA | MALAYSIA

University of Nottingham Ningbo China, 199 Taikang East Road, Ningbo, 315100, China

First published 2021

University of Nottingham
UK | CHINA | MALAYSIA

Novel two-stage fluidized bed-plasma gasification integrated with SOFC and chemical looping combustion for the high efficiency power generation from MSW: A thermodynamic investigation

Peng Jiang [a,b], Ashak Mahmud Parvez [c], Yang Meng [a], Xinyue Dong [a], Mengxia Xu [a,d], Xiang Luo [a,d], Kaiqi Shi [a,d], Tao Wu [a, d,*]

[a] Department of Chemical and Environmental Engineering, The University of Nottingham Ningbo China, Ningbo 315100, China

[b] Shenzhen Gas Corporation Ltd., Shenzhen 518040, China

[c] Institute of Combustion and Power Plant Technology (IFK), University of Stuttgart, Pfaffenwaldring 23, D-70569 Stuttgart, Germany

[d] Key Laboratory for Carbonaceous Wastes Processing and Process Intensification Research of Zhejiang Province, The University of Nottingham Ningbo China, Ningbo 315100, China

[*]Corresponding author: Tao Wu, Tao.Wu@nottingham.edu.cn

Abstract

A novel municipal solid waste (MSW)-based power generation system was proposed in this study, which consists of a bubbling fluidized-bed (BFB)-plasma gasification unit, a high-temperature solid oxide fuel cell (SOFC), a chemical looping combustion (CLC) unit and a heat recovery unit. Process simulation was conducted using Aspen Plus^{TM} and validated by literature data. The energetic and exergetic assessment of the proposed system showed that the net electrical efficiency and exergy efficiency reached 40.9 % and 36.1 %, respectively with 99.3 % of carbon dioxide being captured. It was found that the largest exergy destruction took place in the BFB-Plasma gasification unit (476.5 kW) and accounted for 33.6 % of the total exergy destruction, which is followed by the SOFC (219.1 kW) and then CLC (208.6 kW). Moreover, the effects of key variables, such as steam to fuel ratio (STFR), fuel utilization factor (U_f), current density and air reactor operating temperature, etc., on system performance were carried out and revealed that the system efficiency could be optimized under STFR = 0.5, U_f = 0.8 and air reactor operating temperature of 1000 °C. Furthermore, the

proposed process demonstrated more than 14% improvement in net electrical efficiency in comparison with other MSW incineration and/or gasification to power processes.

Keywords: MSW; bubbling fluidized-bed-plasma gasification; thermodynamic analysis; solid oxide fuel cell; chemical looping combustion

Nomenclature		*W*	Power, kW
ΔG^0	Gibbs free energy at standard pressure and temperature, J mol^{-1}	Abbreviations	
A_a	Active surface area, m^2	AR	Air reactor
$C_{10}H_8$	Naphthalene	ASU	Air separation unit
C_2H_6	Ethane	BFB	Bubbling fluidized-bed gasifier
C_3H_6	Propene	CC	Combined cycle
C_3H_8	Propane	CLC	Chemical looping combustion
CH_4	Methane	FR	Fuel reactor
CO	Carbon monoxide	GT	Gas turbine
CO_2	Carbon dioxide	HE	Heat exchanger
E	Cell voltage, V	HRSG	Heat recovery and steam generation
E_0	Nernst voltage, V	LCA	Life cycle analysis
ER	Equivalence ratio	LHV	Lower heating value
Ex	Exergy, J mol^{-1}	MSW	Municipal solid waste
F	Faraday's constant, C mol^{-1}	RDF	Refused derived fuel
H_2	Hydrogen	SOEC	Solid Oxide Electrolyser Cell
H_2S	Hydrogen sulfide	SOFC	Solid oxide fuel cells
I	Current, A	ST	Steam turbine

i	Current density, A m^{-2}	VOC	Volatile organic compounds
m	Mass flow rate, kg s^{-1}	*Greek symbols*	
n	Molar flow rate, mol s^{-1}	β	Coefficient
Ni	Nickle	η	Efficiency
NiO	Nickle oxide	*Subscripts*	
NO	Nitric Oxide	act	Activation polarization
NO_2	Nitrogen dioxide	com	Concentration polarization
R	Universal gas constant, J $mol^{-1}K^{-1}$	DC	Power generated by the SOFC
S	Sulfur	en	Energy
SO_2	Sulfur dioxide	ex	Exergy
STFR	Steam to fuel mass ratio	ohm	Ohmic polarization
T	Temperature, ^oC	react	Reacted molar flow rate of the gas species
U_f	Fuel utilization factor		

1. Introduction

The generation of solid wastes along with the economic development has become an environmental challenge in the 21st century. In China, the municipal solid waste (MSW) production in the 214 major cities rised from 168.1 million tons in 2014 to 235.6 million tons in 2020 [1]. Although the percentage of MSW being treated has reached 99.7 wt% in 2020 in China, landfill and incineration still account for 45.6 wt% and 50.6 wt% of the treated MSW, respectively [2], which are also associated with environmental issues, such as the emission of uncontrolled greenhouse gases, ground water and soil pollution, and the release of gaseous carcinogens [3]. Besides, the energy efficiency of incineration technology is normally low while the cost is high, which render it less

economically viable. Thus, the development of energy-efficient and environmental-friendly alternatives to enhance MSW energy recovery is of great importance.

Gasification technology is of great potential in the treatment of MSW with less pollution and higher efficiency as compared with conventional MSW treatment technologies. In addition, ,it could generate syngas that could be used in the synthesis of a variety of products [4, 5]. Compared with other types of gasifiers, bubbling fluidized-bed gasifiers (BFB) have excellent heat and mass transfer capacity and can be used to handle a wide range of feedstocks [6, 7]. The operating temperature of BFB gasifiers is usually less than 900 ℃, which allows the discharge of slag in solid state. These characteristics make BFB gasifiers a suitable option for the gasification of MSW [6]. However, a major challenge in the BFB gasification of MSW is the generation of high content of tar (up to 11.2% of the total produced gas) [8]. But the emerging of plasma gasification provides another viable option for the thorough conversion of MSW to high quality syngas with low levels of pollutants under extreme high temperature (up to 5000 ℃) [9-11]. Nevertheless, it was estimated that the electricity consumption of the plasma torch accounts for about 32% of the total energy contained in MSW for a stand-alone plasma gasification [12]. Therefore, there is a need for the development of a novel plasma gasification technology to realize the tar-free syngas generation at relatively low power consumption to improve the economy of the MSW treatment process.

Recently, a demonstration plant, which employed a BFB gasifier to gasify refused derived fuels (RDF) at 650-800 ℃ followed by a plasma converter operating at 1200 ℃, was commissioned [13] and showed that tar was completely converted to syngas and the carbon conversion efficiency was raised to be over 96.9%, which is higher than the efficiency of a single-stage BFB gasification (80-92%) [14]. Im et al. [15] experimentally investigated the syngas production behaviors fed by high density

polyethylene (HDPE) under a gasification-plasma hybrid system operating at 623 °C and found that syngas composition and yield were enhanced compared with those of the conventional fluidized bed gasification. Lately, Evangelisti et al. [16] conducted a life cycle analysis (LCA) of an integrated gasification and plasma cleaning process for power generation. The net electricity efficiency was found to change in the range of 20 to 35% for different waste feedstock.

Solid oxide fuel cells (SOFC) are efficient energy conversion devices that directly produce electricity from fuel gases via electrochemical reactions [17]. The SOFC typically operates at a temperature between 500 and 1000 °C and the maximum theoretical efficiency can reach up to 60% [18]. The integration of coal and/or biomass gasification with SOFC to achieve high energy efficiency has been extensively studied [19-21]. However, studies on the SOFC based power generation system driven by MSW gasification are rarely reported. Galeno et al. [22] designed a RDF plasma gasification system integrated with a SOFC power generation unit and showed that this integrated system had a net power efficiency of 33%. Recently, Perna et al. [9] proposed two novel configurations that combined a waste to energy scheme together with an electric storage system. Thermodynamic analyses suggested that the power generation efficiency was in the range of 35-45% and the energy storage efficiency was 72-92%.

In addition, the chemical looping combustion (CLC) has attracted increasing attentions as an effective and inherent CO_2 mitigation strategy without extra energy penalty [23], which could also lead to the reduction of NO_x emission and exergy losses [24, 25]. The applications of CLC in power plants have been tried with a wide spectrum fuels including natural gas, coal and/or biomass derived syngas [24, 26, 27].

82 However, to the best of our knowledge, no attempt has been made so far to integrate SOFC and
83 CLC with BFB-plasma gasification for highly efficient power production as well as CO_2 capture.
84 Therefore, this work is set out to study the feasibility of such a novel process and to gain insights of
85 its thermodynamic performance.

86 ***2. System description***

87 Fig.1 shows the schematic of the proposed BFB- plasma gasification of MSW that is integrated
88 with SOFC and CLC for highly efficient power generation and CO_2 capture.

89 As shown in Fig.1, such a process consists of four main sub sytems, namely BFB-plasma gasification,
90 solid oxide fuel cell, chemical looping combustion and heat recovery and steam generation (HRSG)
91 together with combined cycle (CC). Solid waste is initially converted to raw syngas containing tar and
92 condensable contaminants in the bubbling fludized bed gasifier using steam and oxygen as the
93 gasification agent. The raw syngas is then treated in the plasma converter to crack tar and organic
94 containiments into small molecules. After the hot gas cleaning, the syngas from the plasma converter
95 is fed to the SOFC, in which the syngas is directly reacted with O^{2-} to generate electricity. At the
96 downstream of the SOFC, the anode gas and depleted air are directed to the fuel reactor and air
97 reactor, respectively, and burned. Then, the flue gas from the chemical looping system is processed
98 in HRSG to recovery heat. The detailed configuration of the proposed process is illustrated in Fig.2.
99 The detailed description of each subsystem is presented in following sections.

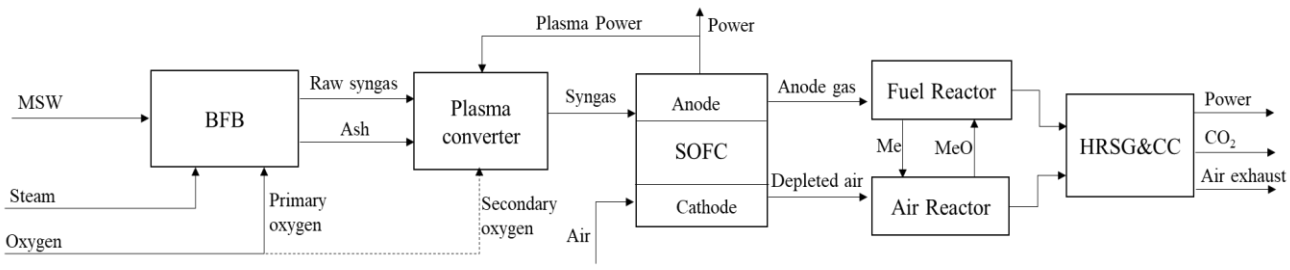

100

Fig.1. Schematic of the proposed BFB- plasma gasification of MSW integrated with SOFC and CLC for power generation and CO_2 capture.

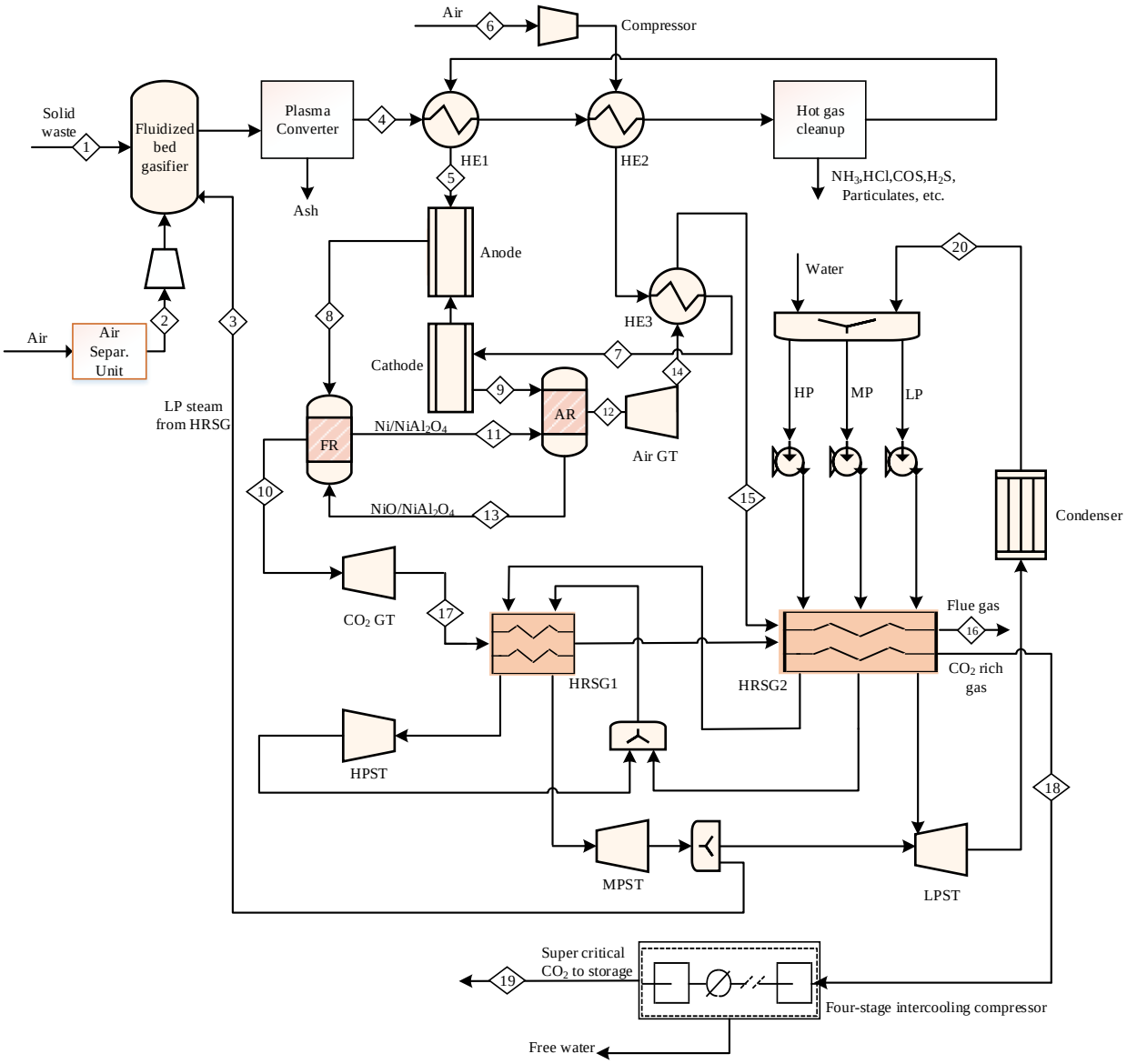

Fig.2. Detailed configuration of the proposed process.

2.1 BFB- plasma gasification

The pre-treated MSW is crushed into 10 to 25 mm and fed into the fluidized-bed gasifier together with oxygen and steam. The amount of oxygen and steam is controlled to maintain autothermal state with the operating temperature in the range of 650 to 800 ^{o}C and to achieve a higher carbon

conversion [8, 28]. A higher gasification temperature is beneficial for the promotion of syngas yield but is also associated with a higher mineral melting possiblity that leads to the agglomeration and defluidization of the gasifier, which subsequently causes the blocakge accident. In this study, the oxygen equivalence ratio (ER) and steam to fuel mass ratio (STFR) are adopted to quantify the feeding rate of the gasification agent. The ER and STFR parameters can be calculated as follows:

$$ER = \frac{(n_{O_2}/n_{MSW})}{(n_{O_2}/n_{MSW})_{stoic}} \quad (1)$$

$$STFR = \frac{m_{steam}}{m_{MSW}} \quad (2)$$

Oxygen needed for the fluidized-bed gasifiction is supplied from a cryogenic air separation unit (ASU), while steam is extracted from the HRSG. In the gasifier, carbon, oxygen and steam are contacted and reacted intensively to convert the solid into syngas. The detailed chemcial reactions in the gasifer can be referred in [29] .The crude gas from the gasifier mainly contains CO,CO_2,CH_4, H_2O and H_2 in conjunction with a certain amount of tar and char. Besides, ash and inorganic material can also be brought out with the raw syngas. Then, the crude gas is sent to the readily-controllable plasma converter where complex organics are exposed to the ultra violet light induced by a carbon plasma electrode and cracked into CO and H_2 at the uniform temperature of 1200 ℃. At the same time, particulate materials in the raw gas enters to the centrifugal designed plasma converter where they are converted into molten slag. The outlet syngas exits the plasma converter and is cooled in the heat exchangers (HE1 and HE2) followed by a gas cleaning unit, in which the contaminates and sulphide are removed by a ceramic filter and a sorbent bed respectively [9, 22]. The clean syngas is heated up and fed to the SOFC subsystem. Table 1 illustrates the ultimate and proximate analysis of the selected minicipal solid waste employed in this study. The main operating conditions of the two stage fluidized-bed plasma gasification subsystem are shown in Table 2.

Table 1

Ultimate and proximate analyses of the selected solid waste (as received) [8].

Ultimate analysis (wt%)		Proximate analysis (wt%)	
C	41	Moisture	14.9
H	5.7	Volatile	59.6
N	1.2	Fixed carbon	6.4
S	0.2	Ash	19.1
O (by difference)	17.5	LHV(dry basis,MJ/kg)	19.99

Table 2

Main operating parameters and assumptions for the two-stage fluidized-bed plasma gasification unit [8, 30, 31].

Unit	Specification
Feedstock	Inlet temperature: 25 ℃
	Mass flow rate : 0.117 kg/s
ASU	Air composition: N_2 (79 vol%)+O_2 (21 vol%)
	Oxygen purity: 95%
	Power consumption:0.325 kWh/kg O_2
	O_2 delivery pressure: 4 bar
Fluidized bed gasifier	Operating pressure: 3.5 bar

	Operating temperature: 800 ℃
	ER:0.37
	STFR:0.2-0.6
	Heat loss: 2.5% HHV fuel
Plasma converter	Operating temperature: 1200 ℃
	Operating pressure:3.25 bar
	Slag cooling method: water
	Total carbon conversion: 96.9%

2.2 Solid oxide fuel cell

In this study, the clean syngas that consists of CO, H_2 and CH_4 is used as the feedstock to the SOFC system. At the anode side of the SOFC, H_2 is considered as the only fuel participating the electrochemical reaction with O^{2-}. This assumption is reasonable since water shift reaction ($CO + H_2O \rightleftharpoons CO_2 + H_2$) and methane steam reaction ($CH_4 + H_2O \rightleftharpoons CO + 3H_2$) take place very fast at high temperatures and are shifted to the right side as hydrogen is consumed [9]. Table 3 shows the main operating parameters and assumptions for the SOFC subsystem.

The power generated by the SOFC is calculated by the multiply of cell voltage (*E*) and current (*I*) which is presented as follows:

$$W_{DC} = E \times I \quad (3)$$

148 The cell voltage (E) is calculated by the difference between ideal Nernst voltage (E_0) and the
149 voltage losses including ohmic polarization (E_{ohm}), activation polarization (E_{act}) and concentration
150 polarization (E_{con}). The equation of *E* is expressed as [32]:

151 $$E = E_0 - E_{ohm} - E_{act} - E_{con} \quad (4)$$

152 The equation for the calculation of Nernst voltage is defined as [33]:

153 $$E_0 = -\frac{\Delta G^0}{2F} + \frac{RT}{2F} ln\left(\frac{p_{H2} p_{O2}^{1/2}}{p_{H2O}}\right) \quad (5)$$

154 where ΔG^0 (J/mol) stands for the molar free Gibbs energy change for the H_2 electrochemical
155 reaction. *F* is the Faraday's constant, *F*= 96 485 C/mol. *T* (K) is the average temperature of the SOFC
156 stack. R represents universal gas constant, *R*=8.314 J/(mol·K). p_{H2}, p_{O2}, p_{H2O} are the partial
157 pressures of average H_2, O_2, H_2O in the anode side of the SOFC.

158 The molar Gibbs free energy change ΔG^0 is correlated with average operating temperature of
159 SOFC using the following equation [32]:

160 $$\Delta G^0 = 0.005275T^2 + 44.28T - 242200 \quad (6)$$

161 While the detailed expressions for voltage losses of E_{ohm}, E_{act}, E_{con} due to the resistance of
162 electrolyte, slow reaction rate on the electrodes and mass transfer limitations in the porous
163 electrodes can be referred to [34].

164 The current of the SOFC generated is calculated by [34]:

165 $$I = 2FU_f(n_{H2} + n_{CO} + 4n_{CH4}) \quad (7)$$

166 where n_{H2}, n_{CO}, n_{CH4} are the molar flow rate supplied to the SOFC. U_f represents the fuel
167 utilization coefficient and the equation is expressed as [32]:

168 $$U_f = \frac{(n_{H2}+n_{CO}+4n_{CH4})_{\text{react}}}{(n_{H2}+n_{CO}+4n_{CH4})} \quad (8)$$

Where the subscript 'react' represents the reacted molar flow rate of the gas species in the SOFC cell.

The current density (i, A/cm^2) is obtained by the total current (I) divides by the active surface area (A_a).

$$i = \frac{I}{A_a} \tag{9}$$

The inverter efficiency for DC to AC conversion is assumed to be 95% [35]. Thus, the actual power output from SOFC is expressed by:

$$W_{\mathrm{SOFC}} = 0.95 W_{DC} \tag{10}$$

Table 3

Main operating conditions and assumptions of the SOFC [18, 19, 35, 36].

Unit	Specification
Operating temperature	900 °C
Operating pressure	3.25 bar
Fuel utilization factor	0.65-0.9
Current density	1000-3500 A/m^2
Air utilization factor	0.182
DC to AC inverter efficiency	0.95
Pressure drop	3% of the inlet pressure
Anode material	Ni/GDC
Cathode material	LSM-YSZ
Electrolyte material	YSZ

2.3 Chemical looping combustion

As mentioned above, the CLC subsystem comprises a fuel reactor (FR) and an air reactor (AR). In the FR, the unconverted syngas from anode side of SOFC reacts with the oxygen carrier which provides the lattice oxygen and completely convert into CO_2 and H_2O. In the AR, the depleted air composed of O_2 (17 vol%) and N_2 from the cathode side of SOFC contacts with the reduced oxygen carrier to realize the complete regeneration of oxygen carrier. The circulating oxygen carrier chosen in the study is NiO/Ni with supported by the inert material of $NiAl_2O_4$ to improve its mechanical behavior [37]. The reactions taken place in the CLC are referred as following equations [30]:

$$CO + NiO \rightarrow CO_2 + Ni, \ \Delta H_{298.15K} = -43.1 \text{ kJ/mol} \quad (11)$$

$$H_2 + NiO \rightarrow H_2O + Ni, \ \Delta H_{298.15K} = -2.1 \text{ kJ/mol} \quad (12)$$

$$CH_4 + 4NiO \rightarrow CO_2 + 2H_2O + 4Ni, \ \Delta H_{298.15K} = 156.5 \text{ kJ/mol} \quad (13)$$

$$Ni + O_2 \rightarrow NiO, \ \Delta H_{298.15K} = -479.4 \text{ kJ/mol} \quad (14)$$

The main operating conditions and assumptions for the CLC subsystem is presented in Table 4. In order to control temperature in the air reactor, excessive air cooling approach is employed as cooling agent to avoid agglomeration of oxygen carriers.

Table 4

Main operating conditions and assumptions of CLC subsystem [18, 30, 38].

Unit	Specification
Fuel reactor	Operate adiabatically
	Operating pressure: 3.15 bar
	$NiO/NiAl_2O_4$ molar ratio : 0.25
	Excess ratio of NiO: 0.2

Air reactor	Operating temperature: 850-1100 °C (air cooling)
	Operating pressure: 3.15 bar
	Pressure drop: 10%

2.4 HRSG and combined cycle

The effluent gases from the FR and AR are at high temperature and pressure states and they are directly sent to the CO_2 gas turbine and air gas turbine for the additional power generation. Then, the gases from the two turbines are forwarded to HRSG unit to recovery heat for steam generation. The different pressure steam streams produced from the HRSG are led to steam turbines for power generation. After the heat recovery in HRSG, the stream initially from FR is cooled to 30 °C and water is separated from this stream. The CO_2 rich stream is then directed to a four-stage intercooled compressor to the pressure of 120 bar which is ready for the pipeline transportation. Table 5 presents the main specifications adopted in this subsystem.

Table 5

Main operating parameters and assumptions in the HRSG & GT/ST subsystem [39].

Unit	Specification
Air gas turbine	Discharge pressure:1.01 bar
	Isentropic efficiency: 88%
	Mechanical efficiency: 99%
CO_2 gas turbine	Discharge pressure:1.01 bar
	Isentropic efficiency: 88%
	Mechanical efficiency: 99%

HRSG & CC	Pinch temperature: 10 ℃
	Pressure loss: 8%
	HP steam:120 bar
	MP steam:30 bar
	LP steam:4 bar
	Condenser pressure: 0.05bar
	Steam turbine isotropic efficiency:88%
	Steam turbine mechanical efficiency: 99%
	Reheated temperature: 540 ℃

3. Methodology

3.1 Simulation

The complete process shown in Fig. 2 is simulated using the Aspen Plus™ software [40, 41]. The global physical properties are calculated using Peng-Robinson equation. The MSW and ash are considered as non-conventional components in the Aspen Plus™. The other components such as CO, H_2, H_2O, CO_2, C_2H_6, C_3H_6, C_3H_8, O_2, N_2, S, H_2S, SO_2, NO, NO_2, et al., are treated as conventional species, while carbon, Ni, NiO, $NiAl_2O_4$ are classified as the solid type. Since tar is a commonly seen complex substance generated during gasification, during the simulation, naphthalene ($C_{10}H_8$) is used as the representative.

The simulation of BFB- plasma gasification subsystem mainly includes two reactors, namely a fluidized-bed reactor and a plasma converter. In the fluidized-bed reactor, the solid fuel is initially pyrolyzed into gases and char and then the gases and char are gasified under the gasification agent

of oxygen and steam. The built-in reaction modules of RYield, RStoic and RGibbs are adopted to simulate solid waste pyrolysis, hydrocarbons conversion and tar formation, and equilibrium gasification with oxygen and steam respectively [42]. Several correlation equations which connect the hydrocarbons conversion (CH_4, C_2H_4, C_2H_6, C_3H_6, C_3H_8 and $C_{10}H_8$) with gasification temperature are incorporated in Aspen Plus using Fortran codes [43, 44]. Besides, the carbon conversion is also controlled by Fortran code. The simulation of plasma converter is based on RGibbs module in which all the reactions are considered to reach an equilibrium state at the plasma induced temperature of 1200 ^{o}C. The simulated syngas compositions are compared with the experimental values carried out by Materazzi et al. [8]. The clean-up section is simulated as a black-box where the separation efficiencies of each component are assumed.

The simulation of anode and cathode in the SOFC are based on RGibbs module and Sep module, respectively. The O_2 split ratio in the cathode is controlled by using a Calculator based on the U_f. Besides, the air inlet molar flow is calculated using a Design-Spec block according to the oxygen consumption. In addition, another Calculator block is incorporated in the Aspen Plus to compute the Nernest voltage, voltage losses due to polarizations, current, and electricity power according to the Eq. (5) to Eq. (12).

For the simulation of chemical looping combustion subsystem, the RGibbs and SSplit are adopted as modules to model the fuel and air reactors, gases and oxygen carrier separation, respectively. The air turbine, CO_2 turbine and steam turbine are simulated as the Comp module with the selection of turbine sub-option. The HRSG is modeled using MheatX module whereas the heat exchangers are shifted to the HeatX module.

3.2 Thermodynamic performance indicators

The overall net electrical efficiency (η_{en}) of the proposed process is expressed as [36]:

$$\eta_{\mathrm{en}} = \frac{W_{\mathrm{SOFC}}+W_{\mathrm{GT}}+W_{\mathrm{ST}}-W_{\mathrm{pump}}-W_{\mathrm{ASU}}-W_{\mathrm{compressor}}-W_{\mathrm{plasma}}}{m_{\mathrm{MSW}}\cdot \mathrm{LHV}_{\mathrm{MSW}}} \quad (15)$$

where the subscripts of SOFC, GT, ST, pump, ASU, compressor, and plasma indicate the SOFC, gas turbines, steam turbines, pumps, air separation unit, syngas compressor, and plasma torch respectively.

The exergy balance of an individual system is expressed as [45]:

$$\sum EX_{in} = \sum EX_{out} + EX_{des/loss} \quad (16)$$

where the $\sum EX_{in}$ denotes the overall input exergy including chemical exergy, physical exergy and heat exergy; and $EX_{des/loss}$ denotes the exergy destruction due to irreversibility and loss. The calculation expressions of chemical and physical exergy of conventional streams and heat exergy can be seen elsewhere [46].

The overall exergy efficiency of the process is calculated as:

$$\eta_{ex} = \frac{W_{\mathrm{SOFC}}+W_{\mathrm{GT}}+W_{\mathrm{ST}}-W_{\mathrm{pump}}-W_{\mathrm{ASU}}-W_{\mathrm{compressor}}-W_{\mathrm{plasma}}}{\mathrm{EX}_{\mathrm{MSW}}+\ \mathrm{EX}_{\mathrm{water}}+\ \mathrm{EX}_{\mathrm{air}}} \quad (17)$$

where $\mathrm{EX}_{\mathrm{MSW}}$ is chemical exergy of MSW which can be deduced according to a common exergy formula (O/C mass ratio ≤2) as follows [47]:

$$\mathrm{EX}_{\mathrm{MSW}} = \beta m_{\mathrm{MSW}} \cdot \mathrm{LHV}_{\mathrm{MSW}} \quad (18)$$

$$\beta = \frac{1.044+0.016\frac{h}{c}-0.3496\frac{o}{c}\left(1+0.0531\frac{h}{c}\right)+0.0493\frac{n}{c}}{1-0.4124\frac{o}{c}} \quad (19)$$

where *h*, *c*, *o*, *n* stand for the mass fraction of H, C, O, N in the solid waste (see Table 1), respectively.

4. Results and discussion

4.1 Model validation

Fig. 3 presents the comparison of the outlet gas composition of this study against experimental values and modelling results reported by Materazzi et al. [8]. For the BFB gasifier outlet gas composition (Fig. 3a), the current simulation is closer to experimental results. Besides, the current simulation of the gas compostion at the outlet of the plasma coverter is totally consistent with the results of the experiment (Fig.3b). As the outlet syngas from the converter is fed to the downstream system for furthur processing, the constructed model for the simulation of BFB- plasma gasification is appropriate and can be employed to predict the syngas performances. It is also clear from Fig. 3 that the H_2 and CO contents increased to 32.2 and 26.8%, respectively, after the processing of the converter. Simultaneously, the water and volatile organic compounds (VOC) decreases to 29.71 and 0.63%, respectively. This can be attributed to the enhanced endothermal reactions of hydrocarbon steam reforming at 1200 ℃ enabled by the plasma torch.

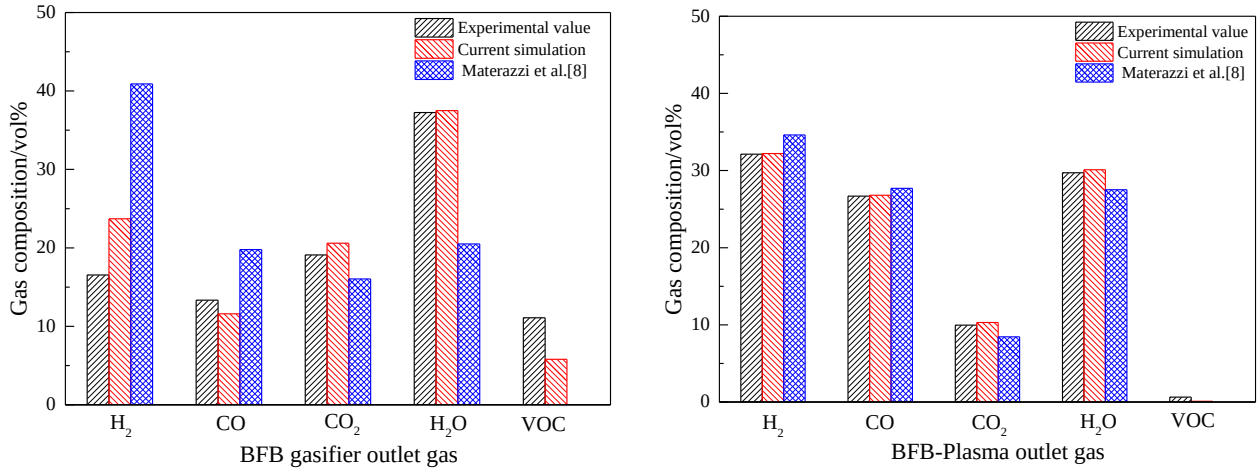

Fig.3. Comparison of the outlet gas composition of current simulation values with experimental data and modelling results of Materazzi et al. [8]. Simulation condition: Feedstock: 50kg/h; ER:0.37.

The aforementioned SOFC model is validated by the comparison between literature data and current simulation values regarding the anode inlet gas, anode outlet gas, voltage, current density and gross efficiency at same operating conditions referred in [34, 48]. As shown in Table 6, a good agreement is achieved between our simulation data and reported value. The deviation is found to be in the range of 0 to 5.8%, which indicates the SOFC model developed in this study is reliable.

Table 6

Comparison the SOFC simulation values with literature data.

Item	Literature value [34]	Current simulation	Error/%
Anode inlet gas/ vol%			
H_2	26.9	27.4	1.85
CO	5.6	5.7	1.78
CH_4	10.4	9.8	5.77
H_2O	27.8	27.9	0.36
CO_2	23.1	23.2	0.43
N_2	6.2	6.1	1.61
Anode outlet gas/ vol%			
H_2	11.6	11.6	0
CO	7.4	7.4	0
H_2O	50.9	50.9	0
CO_2	24.9	25	0.4
N_2	5.1	5.1	0
Voltage/V	0.683	0.692	1.32

Current density/(A/m^2)	1821	1804	0.93
SOFC gross efficiency/%	51.28	51.58	0.58

Table 7 lists dry gas composition at the outlet of FR for both simulation values and experimental data at the operating temperature of 700 and 800 ℃. The experiment was carried out in a 10 kW CLC plant with natural gas as the fuel and $NiO/NiAl_2O_4$ as the oxygen carrier [49]. As indicated in Table 7 that the simulation value is nearly identical to the experimental data and the relative difference is very small (<10%) which shows the simulation methodology of CLC is appropriate/acceptable.

Table 7

Comparison of the dry gas composition at the outlet of FR between the simulation values and experimental data.

Syngas composition/vol%	T_{FR}:700 ℃			T_{FR}:800 ℃		
	Experimental	Simulation	Error/%	Experimental	Simulation	Error/%
CO_2	94.47	95.3	0.9	96.41	96.3	0.1
CO	1.32	1.2	9.1	1.11	1.1	0.9
H_2	3.58	3.3	7.8	1.82	1.95	7.1

4.2 Simulation results

The proposed process was simulated according to the basic operating conditions shown in Table 1 to Table 5. At the conditions of STFR =0.5, fuel utilization of 0.8, current density of 2200 A/m^2 and operating temperature of AR of 1000 ℃, the simulation results, such as temperature, pressure, mass flow and molar composition for the key state points (see Fig.2), are listed in Table 8.

To improve power generation efficiency of the HRSG & CC subsystem, pinch analysis was conducted by adjusting the steam flow rates of high pressure, medium pressure and low pressure to construct the hot and cold composite curves with a minimum approach temperature of 10 ℃. Fig.4 presents heat composite curves for HRSG2. As can be observed from this figure that the maximum heat recovered from the stream of 15 and 18 is about 782 kW. The pinch point shows up at the heat duty of 156 kW and the corresponding temperature of 145 ℃, which represents the initial evaporation temperature (bubble point) of the low-pressure steam.

Table 8

Key flow streams of the proposed process.

Flow no.	Temperature	Pressure	Mass flow	molar composition								
	[C]	[Bar]	[kg/h]	H_2	CO	CO_2	N_2	O_2	H_2O	NiO	Ni	$NiAl_2O_4$
1	25	1.00	421.2									
2	25	1.00	209.9				0.05	0.95				
3	283.9	4.00	170.0						1.0			
4	1200	3.5	727.0	0.323	0.264	0.099	0.008		0.294			
5	791	3.45	717.8	0.327	0.268	0.1	0.008		0.298			
6	25	1.00	7179.6				0.79	0.21				
7	650	3.45	7179.6				0.79	0.21				
8	900	3.25	1018.8	0.069	0.05	0.317	0.008		0.555			
9	900	3.25	6878.6				0.821	0.179				
10	980.5	2.75	1090.9	0.003	0.002	0.365	0.008		0.622			
11	980.5	2.75	4338.2							0.04	0.16	0.8

12	1000	2.75	6806.5				0.829	0.171			
13	1000	2.75	4410.2							0.2	0.8
14	749.8	1.01	6806.5				0.829	0.171			
15	367.9	1.01	6806.5				0.829	0.171			
16	90	1.01	6806.5				0.829	0.171			
17	800	1.01	1090.9	0.003	0.002	0.365	0.008		0.622		
18	90	1.01	1090.9	0.003	0.002	0.365	0.008		0.622		
19	40	120	647.5	0.007	0.006	0.965	0.022				
20	37.9	0.05	697.0						1		

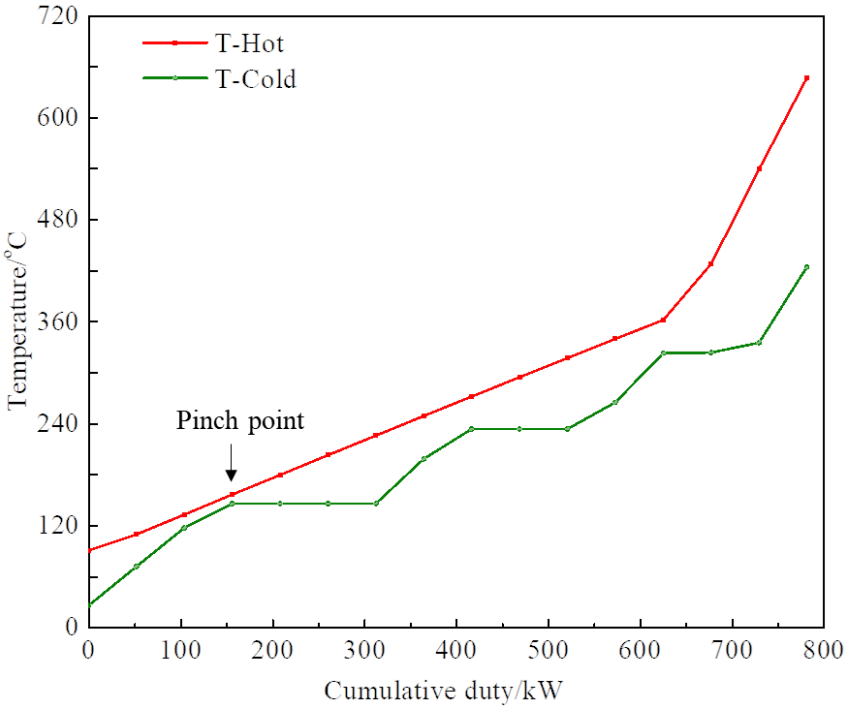

Fig.4. Heat composite curve for the HRSG2

After the pinch analysis, the energy and exergy performances of the proposed process are computed and presented in Table 9. The net electricity generated in this process is 815.7 kW with a

net electrical efficiency of 40.9%. The total exergy fed into the process is 2223.9 kW resulting in the exergy efficiency of 36.7%. It can also be noticed from this table that the electricity generated by SOFC shares largest proportion of the total gross electricity, accounting for 42%. The air gas turbine contributes to 552.3kW electricity due to the expansion of large amount of depleted air.

While from the electricity consumption perspective, the air compression unit takes up largest share of 325.9 kW because of ample air requirements in SOFC unit as the air utilization factor of 18.2% (see Table 3). The electrical consumption of plasma torch is determined to be 226.3 kW which is tantamount to 11.3% of the input LHV of MSW and this proportion decreases significantly in comparison with that of 32% [12] in a stand-alone plasma gasification system. Besides, the CO_2 capture efficiency (defined as the CO_2 molar flow rate in stream 19 to the molar flow rate of both CO and CO_2 in the stream 4) is 99.3% and the CO_2 compression unit consumes about 76.7 kW. The high CO_2 capture efficiency is mainly because of the employment of chemical looping combustion which converts the CO into CO_2 with lattice oxygen provided in NiO in the fuel reactor. In this study, the electricity penalty due to CO_2 capture and compression accounts for approximately 3% which is lower than that of conventional amine CO_2 capture technologies with 8-10% penalty [50].

Table 9

Energy and exergy performance of the proposed process.

Units	Value/kW
Solid waste input (LHV)	1990
SOFC	652.5
CO_2 GT	99.3

Air GT	552.2
HPST	28.9
MPST	84.3
LPST	137.6
Pump	1.86
CO_2 compression	76.7
Air compression	325.9
O_2 compression	9.7
ASU	68.3
Auxiliary	30.5
Plasma consumption	226.3
Net electricity	815.7
Net electrical efficiency, η_{en}/%	40.9
$\mathrm{EX}_{\mathrm{solid}}$	2183.1
$\mathrm{EX}_{\mathrm{water}}$	30.9
$\mathrm{EX}_{\mathrm{air}}$	9.9
Exergy efficiency, η_{ex}/%	36.7
CO_2 capture efficiency/%	99.3

The exergy destruction and exergy efficiency distributions of the key components in the proposed process are presented in Fig. 5(a) and Fig. 5(b), respectively. The exergy destruction for a unit is defined as the difference between inputs exergy and output exergy, while exergy efficiency

for a unit is defined in literature [39]. It can be noticed from Fig. 5(a) that the largest exergy destruction takes place in the BFB-plasma gasification unit (476 kW), which is primarily attributed to the intrinsically irreversible gasification reactions converting from low entropy specie of carbon to high entropy species of syngas. Besides, the unconverted carbon, heat loss and mixture of gasifying agents also contribute to the exergy destruction of gasification unit. The exergy destruction of SOFC is responsible for 219.1 kW mainly caused by the irreversibility of electrochemical reactions. The CLC unit shares about 14.7% of the total exergy destruction due to the unavoidable destroy from chemical reactions. In addition, CO_2 compression unit is moderately occupied 115.6 kW exergy destruction owing to the water separation during cooling and the large electricity input to the compressor of 76.7 kW. The other units of ASU, HRSG2, HE2, Air compressor, HE3 and DC-AC converter are responsible for 68.2, 54.9, 47.6, 43.9, 34.7, 34.2 kW exergy destruction, respectively.

As indicated by Fig. 5(b), the HRSG1 has the highest exergy efficiency of 98.2% due to the small temperature difference in heat transfer. However, the exergy efficiency in HRSG2 is about 86.1 % owing to a large temperature difference between the cold and hot streams. While the largest exergy destruction is detected in CO_2 compression unit, with an exergy efficiency of 67.8%. This is because the separated CO_2 is inherently of high physical exergy at high pressure compared with the state before compression. The exergy efficiencies of reactive units of BFB-plasma gasification, SOFC and CLC are 80.7, 87.7 and 89.1%, respectively. In combination with the findings in Fig.5, to improve the overall exergy efficiency of the entire process, the key is to reduce the exergy destructions of BFB-plasma gasification, SOFC and CLC, which could be achieved via lowering moisture content of MSW, preheating feed gas temperature to close the operating temperature, reducing heat loss of gasifier, and circulating of the anode-off gas to anode.

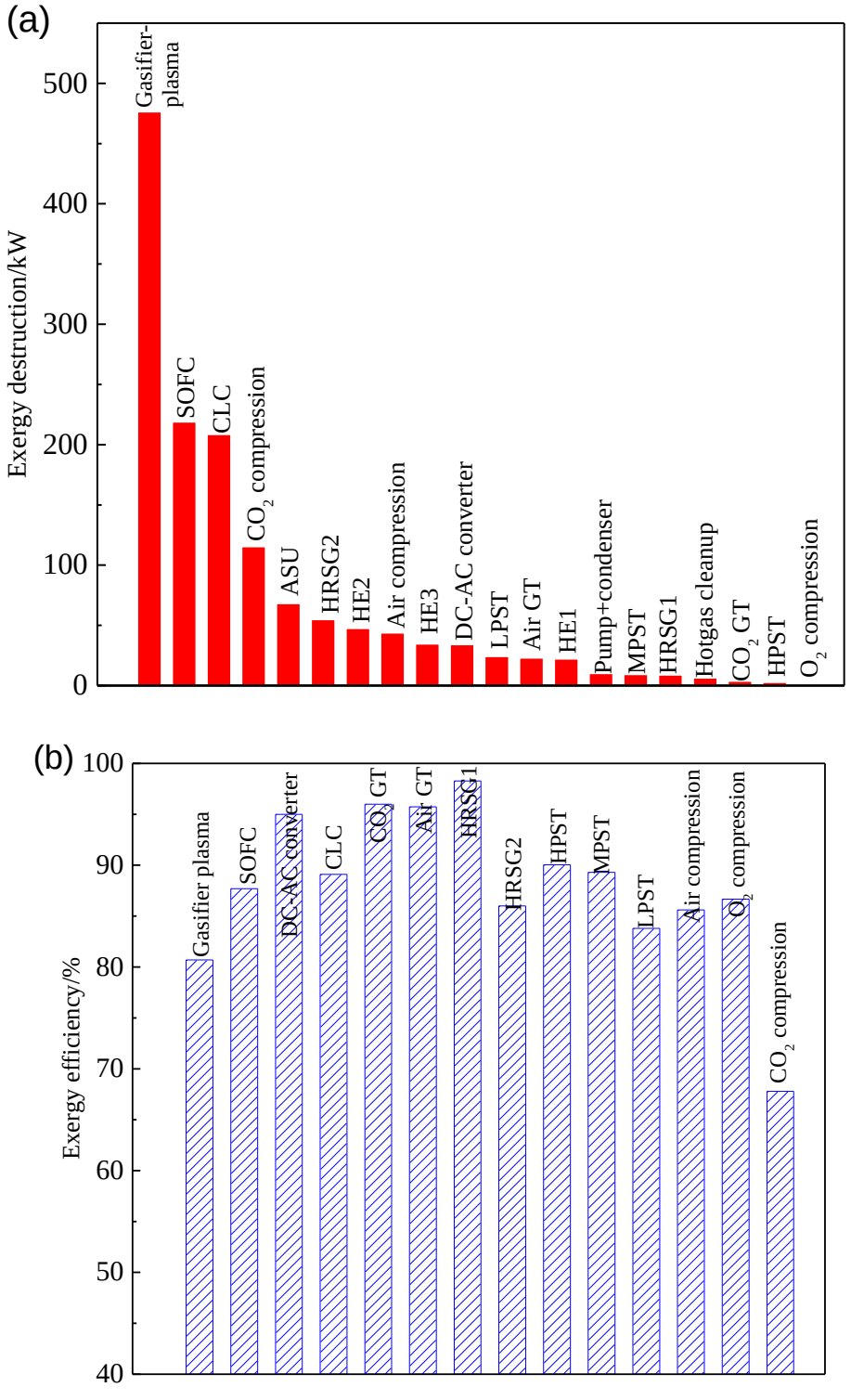

Fig.5. Exergy destruction (a) and exergy efficiency distributions (b) of the key components for the proposed process.

4.3 Sensitivity analysis

In this study, the influences of four key operating parameters, i.e., the steam to fuel ratio, fuel utilization factor, current density and operating temperature, on both energy and exergy efficiencies are examined. Fig. 6 shows the effect of STFR on system efficiency. It can be seen in Fig. 6 that when the STFR increased from 0.2 to 0.6, both the energy and exergy efficiencies show a moderate increase initially, and then decrease, reaching its maximum energy and exergy efficiency of 40.9 and 36.7%, respectively, at STFR =0.5. The injection of steam into the gasifier promotes the carbon conversion ($C+H_2O \rightarrow CO+H_2$), which promotes the increase of the syngas flow rate. Besides, the increment of power generation is larger than the power consumption of plasma unit. Consequently, the power production is enhanced and resulted in the improvement of system performances. However, when STFR is beyond 0.5, further increase of steam requires supplementary energy to maintain the designated gasification operating temperature, leading to the decrease of system efficiencies.

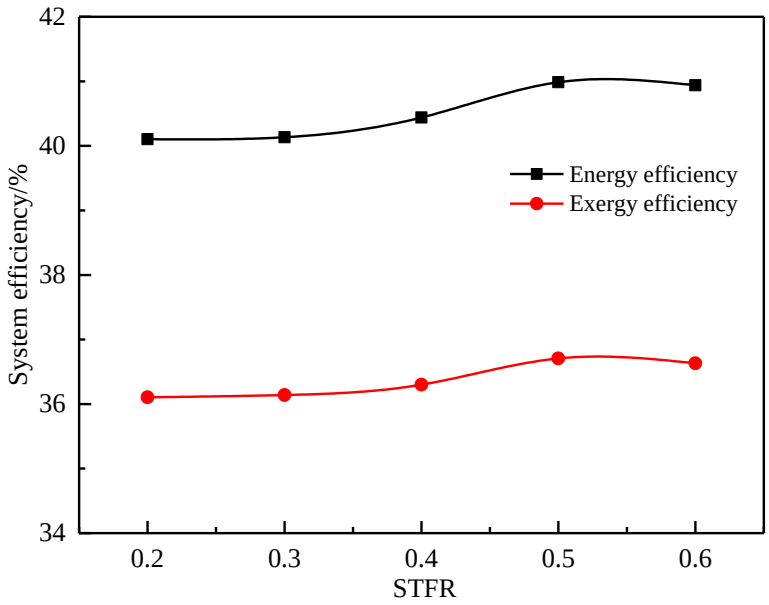

Fig.6. Effect of steam to fuel ratio on system efficiency performance.

The effect of fuel utilization factor on the system efficiencies of the proposed process is shown in Fig.7. As indicated in this figure that increasing fuel utilization factor in SOFC component leads to higher energy and exergy efficiencies and then these efficiencies exhibited a decreasing tendency after U_f is beyond 0.8. At U_f =0.8, the energy and exergy efficiencies are found to be maximum and their corresponding values are 40.9% and 36.7%, respectively. This phenomenon can be explained by the enhancement of electrochemical reaction rates leading to the addition of power output from SOFC when U_f<0.8. Besides, the compression work of air is also promoted as the increase of U_f. However, the increment of power consumption is lower than that of power output. Hence, increment in both energy and exergy efficiency are expected. On the contrary, when U_f is beyond than 0.8, further increase in U_f results in less amount of syngas available in the CLC unit and causes the drop of the combustion temperature correspondingly. Therefore, the decrease of net power generation from GT and ST is the main reason responsible for the reduction of system efficacies.

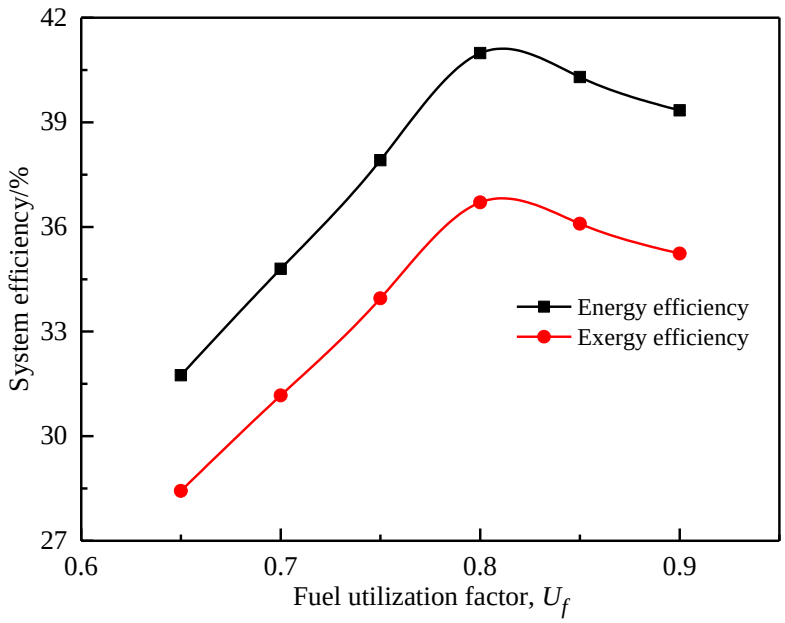

Fig.7. Effect of fuel utilization factor on system efficiency performance.

Fig. 8 illustrates the effect of varying current density from 1000 to 3500 A/m^2 of SOFC on both the overall energy and exergy efficiencies. Referring to Fig.8, with increasing of current density, the energy and exergy efficiencies decrease monotonously from 46.7 to 34.9% and from 41.8 to 31.2%, respectively. This is mainly due to the reduction of cell voltage leading to the decrease of power output from SOFC subsystem when the current density increases [46].

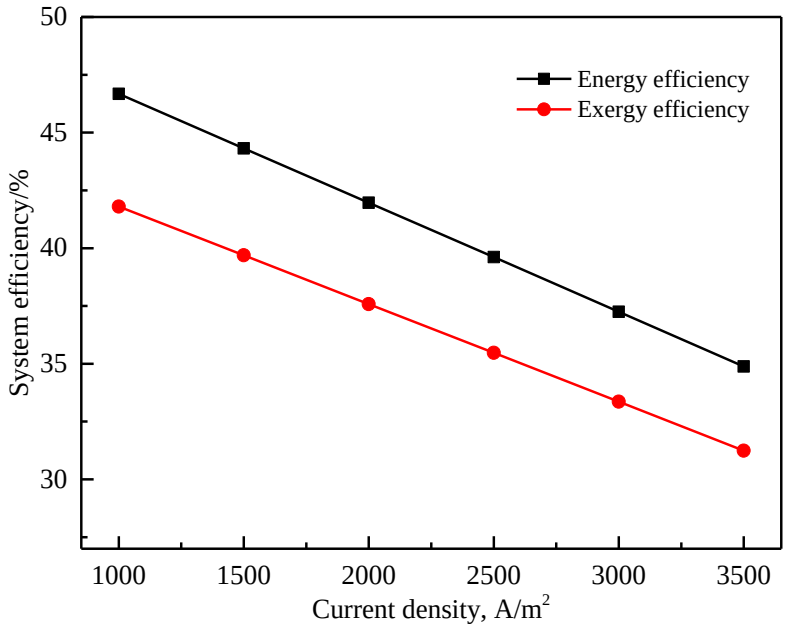

Fig.8. Effect of current density on system efficiency performance.

The effect of changing the air reactor temperature of the CLC on the energy and exergy efficiencies is presented in Fig.9. Based on Fig.9, when the air reactor temperature changes from 850 to 1100 ºC, both of the energy and exergy efficiencies are obtained their respective maximum values of 40.9 % and 36.7 % at the air reactor temperature of 1000 ºC. The increment of system efficiencies derives from the higher inlet temperature of air reactor turbine contributing to a significant increment of net power output [39]. Nevertheless, above 1000 ºC, the efficiencies begin to drop owing to the increase of external energy supplements for the chemical reactions heat generated in AR cannot fully meet the energy requirement to maintain the higher operating temperature.

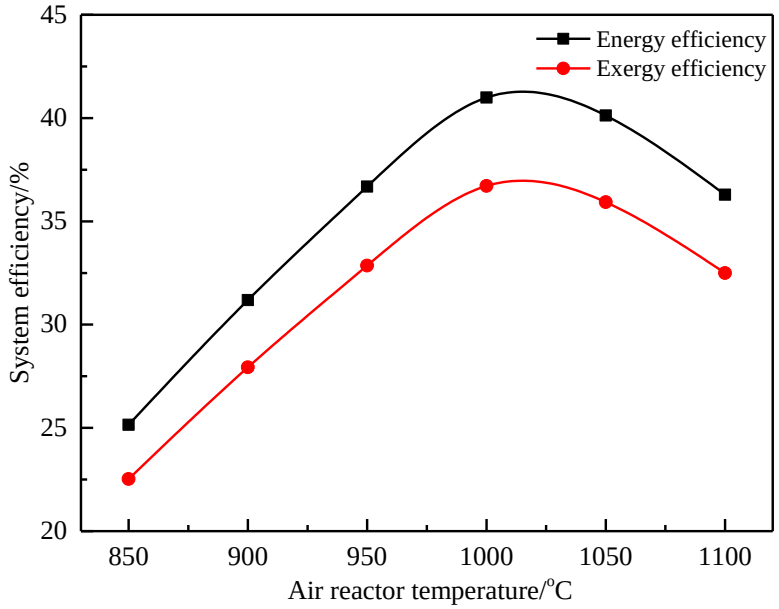

Fig.9. Effect of air reactor temperature on system efficiency performance

4.4 System performance comparison

To evaluate energy recovery level of the proposed system, net energy efficiency is compared with that of MSW to power reported by other researchers. The current study considers six integration power production processes denoted as Case A to F using either combined cycle or SOFC driven by MSW incineration or gasification. The configurations of Case A to F are briefly outlined in the following:

- Case A: Integrating incineration and steam power cycle [29, 51-53]. MSW mixed with air are combusted in the boiler to produce steam. Then, the steam at different pressure levels is employed to boost the steam turbines for power production.
- Case B: Integrating conventional gasification and combined power cycle [53]. MSW is gasified firstly and then the syngas is fed into gas turbines followed by steam turbines.

- Case C: Integrating plasma gasification and combined power cycle [51, 54]. MSW is gasified using plasma torch and afterwards the generated syngas is sent to gas turbines combined cycle.
- Case D: Integrating plasma gasification and SOFC as well as steam power cycle [22]. MSW plasma gasification is integrated with SOFC and followed by a steam cycle.
- Case E: Integrating plasma gasification and SOFC as well as SOEC for power production [9]. MSW plasma gasification with oxygen-rich air or hydrogen and syngas is directed into SOFC for power generation.
- Case F: Integrating BFB-Plasma gasification and combined power Cycle [16]. MSW is gasified in a bubbling fluidized-bed gasifier and then goes to a plasma converter to treatment the syngas. After that, the syngas is travelled to gas turbine combined cycle.
- Present work: Integrating BFB-Plasma gasification and SOFC as well as CLC combined power cycle.

Fig. 10 shows the comparison of net energy efficiency performances for the above cases. As observed from Fig. 10, the incineration system (Case A) has the lowest energy efficiency varied from 15.3 to 21.3%, while the energy efficiency of the integrated conventional gasification system (Case B) with combined cycle reaches 27.2 %. This is mainly due to the combustion of syngas in gas turbine, which produces additional power. Besides, the steam cycle has a higher Carnot energy efficiency of Case B due to higher temperature of flue gas from gas turbines compared with MSW combustion system. For these systems led by one-stage plasma gasification of Cases C, D and E, the highest energy efficiency belongs to the combination of SOFC and SOEC. In addition, the energy efficiency of present work is relative at least 14 % improvement in comparison with that of Case F which also adopts the

same BFB-Plasma gasification technology. The reason of the efficiency increment can be attributed to the application of the energy-efficient SOFC unit. Furthermore, the net energy efficiency of present work is approximately 4% lower than the highest efficiency (44.9%) of Case E which employs pure hydrogen as the plasma gas in the gasification section and that hydrogen is provided by SOEC. However, the calculation of the net electrical efficiency in Case E does not previously include the electrical consumption of the hydrogen generation although the power in SOEC is supplied by a renewable energy of wind. Besides, the involvement of CO_2 capture does not exist in Case E. Hence, it is reasonable to conclude that the proposed process is thermodynamically more performing and can realize low-to-zero CO_2 emission.

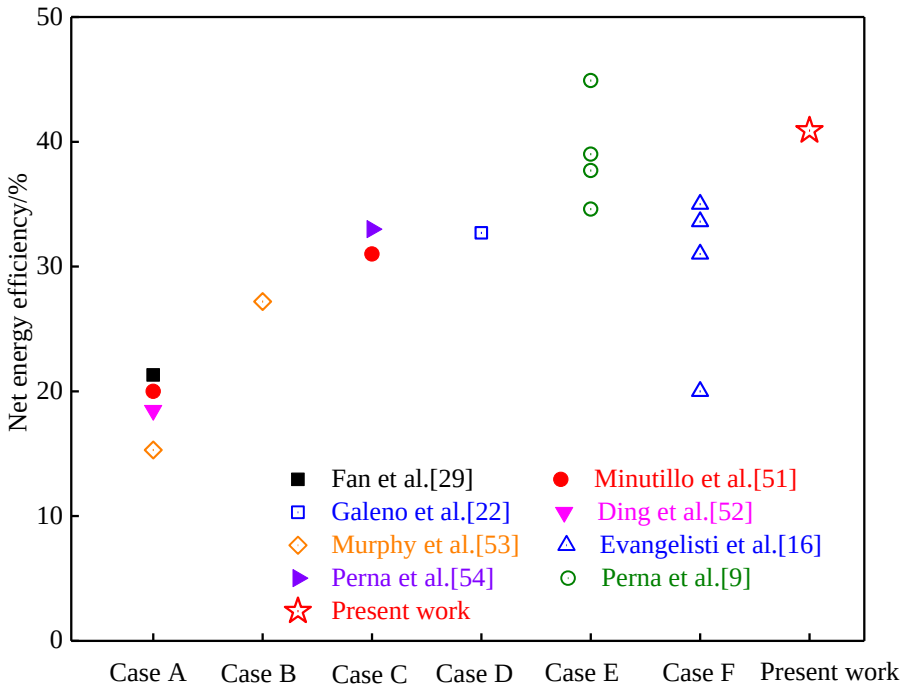

Fig. 10. Comparison of net energy efficiency performances for different MSW combustion or gasification to power configurations

5. Conclusions

In this study, BFB-Plasma gasification, SOFC, CLC and HRSG & CC subsystems are integrated for power generation using MSW as the fuel. Process simulation results showed that the hybrid system could achieve a net electrical efficiency of 40.9 % and an exergy efficiency of 36.7 % with a CO_2 capture efficiency of 99.3 %. Exergy destruction distribution is the largest in BFB-Plasma gasification unit accounting for 33.62 % of the total exergy destruction rates. The SOFC and CLC units are responsible for 15.45 and 14.72 % of the total exergy destruction, respectively. It is found that the optimal operating conditions are STFR = 0.5, utilization factor of 0.8 and operating temperature of CLC as 1000 ℃. Besides, it is revealed that higher current density of SOFC shows a negative impact on system efficiency. In comparison with other MSW to power processes, the proposed process reaches a higher net electrical efficiency.

Acknowledgements

This work is supported by the Ningbo Science and Technologies Innovation 2025 Major Special Project (2018B10027). The Zhejiang Provincial Department of Science and Technology is acknowledged for this research under its Provincial Key Laboratory Programme (2020E10018).

References

1. MOEE, *Annual report on pollution prevention and control of solid waste in large and medium cities in 2020*. 2020, Ministry of Ecology and Environment of China: Beijing.
2. China, N.B.o.S.o. *Urban waste collection and transportation*. 2020 [cited 2021 Feb. 28]; Available from: http://data.stats.gov.cn/index.htm.
3. Hu, M., et al., *Hydrogen-rich gas production by the gasification of wet MSW (municipal solid waste) coupled with carbon dioxide capture.* Energy, 2015. **90**: p. 857-863.

4. Lv, L., Z. Zhang, and H. Li, *SNG-electricity cogeneration through MSW gasification integrated with a dual chemical looping process.* Chemical Engineering and Processing - Process Intensification, 2019. **145**: p. 107665.
5. Couto, N., V. Silva, and A. Rouboa, *Municipal solid waste gasification in semi-industrial conditions using air-CO2 mixtures.* Energy, 2016. **104**: p. 42-52.
6. Lopez, G., et al., *Recent advances in the gasification of waste plastics. A critical overview.* Renewable and Sustainable Energy Reviews, 2018. **82**: p. 576-596.
7. Watson, J., et al., *Gasification of biowaste: A critical review and outlooks.* Renewable and Sustainable Energy Reviews, 2018. **83**: p. 1-17.
8. Materazzi, M., et al., *Performance analysis of RDF gasification in a two stage fluidized bed–plasma process.* Waste Management, 2016. **47**: p. 256-266.
9. Perna, A., et al., *Combining plasma gasification and solid oxide cell technologies in advanced power plants for waste to energy and electric energy storage applications.* Waste Management, 2018. **73**: p. 424-438.
10. Mountouris, A., E. Voutsas, and D. Tassios, *Solid waste plasma gasification: equilibrium model development and exergy analysis.* Energy Conversion and Management, 2006. **47**(13-14): p. 1723-1737.
11. Arena, U., *Process and technological aspects of municipal solid waste gasification. A review.* Waste management, 2012. **32**(4): p. 625-639.
12. Helsen, L. and A. Bosmans. *Waste-to-Energy through thermochemical processes: matching waste with process*. in *Proceedings of the 1st International Academic Symposium on Enhanced Landfill Mining*. 2010. Haletra.
13. Morrin, S., et al., *Two stage fluid bed-plasma gasification process for solid waste valorisation: Technical review and preliminary thermodynamic modelling of sulphur emissions.* Waste Management, 2012. **32**: p. 676-684.
14. Materazzi, M., et al., *Tar evolution in a two stage fluid bed–plasma gasification process for waste valorization.* Fuel Processing Technology, 2014. **128**: p. 146-157.
15. Cho, I.J., et al., *Enhancement of synthesis gas production using gasification-plasma hybrid system.* International Journal of Hydrogen Energy, 2015. **40**: p. 1709-1716.
16. Evangelisti, S., et al., *Integrated gasification and plasma cleaning for waste treatment: A life cycle perspective.* Waste management, 2015. **43**: p. 485-496.
17. Adams, T.A., et al., *Energy conversion with solid oxide fuel cell systems: A review of concepts and outlooks for the short-and long-term.* Industrial & Engineering Chemistry Research, 2012. **52**(9): p. 3089-3111.
18. Chen, S., N. Lior, and W. Xiang, *Coal gasification integration with solid oxide fuel cell and chemical looping combustion for high-efficiency power generation with inherent CO2 capture.* Applied Energy, 2015. **146**: p. 298-312.
19. Thattai, A.T., et al., *Towards retrofitting integrated gasification combined cycle (IGCC) power plants with solid oxide fuel cells (SOFC) and CO2 capture–A thermodynamic case study.* Applied Thermal Engineering, 2017. **114**: p. 170-185.
20. Choudhury, A., H. Chandra, and A. Arora, *Application of solid oxide fuel cell technology for power generation—A review.* Renewable and Sustainable Energy Reviews, 2013. **20**: p. 430-442.
21. Detchusananard, T., et al., *Multi-objective optimization of sorption enhanced steam biomass gasification with solid oxide fuel cell.* Energy Conversion and Management, 2019. **182**: p. 412-429.
22. Galeno, G., M. Minutillo, and A. Perna, *From waste to electricity through integrated plasma gasification/fuel cell (IPGFC) system.* international journal of hydrogen energy, 2011. **36**(2): p. 1692-1701.
23. Zhang, X., et al., *A chemical intercooling gas turbine cycle with chemical-looping combustion.* Energy, 2009. **34**(12): p. 2131-2136.

24. Hossain, M.M. and H.I. de Lasa, *Chemical-looping combustion (CLC) for inherent CO2 separations—a review.* Chemical Engineering Science, 2008. **63**(18): p. 4433-4451.
25. Jin, H., et al., *A new principle of synthetic cascade utilization of chemical energy and physical energy.* Science in China Series E: Technological Sciences, 2005. **48**(2): p. 163-179.
26. Aghaie, M., M. Mehrpooya, and F. Pourfayaz, *Introducing an integrated chemical looping hydrogen production, inherent carbon capture and solid oxide fuel cell biomass fueled power plant process configuration.* Energy Conversion and Management, 2016. **124**: p. 141-154.
27. Fan, L.-S., *Chemical looping systems for fossil energy conversions*. 2011: John Wiley & Sons.
28. Materazzi, M., et al., *Thermodynamic modelling and evaluation of a two-stage thermal process for waste gasification.* Fuel, 2013. **108**: p. 356-369.
29. Fan, J., et al., *Thermodynamic performance of SNG and power coproduction from MSW with recovery of chemical unreacted gas.* Waste Management, 2017. **67**: p. 163-170.
30. Fan, J., et al., *Thermodynamic and environmental evaluation of biomass and coal co-fuelled gasification chemical looping combustion with CO2 capture for combined cooling, heating and power production.* Applied energy, 2017. **195**: p. 861-876.
31. Wan, W., K. Engvall, and W.H. Yang, *Model investigation of condensation behaviors of alkalis during syngas treatment of pressurized biomass gasification.* Chemical Engineering and Processing-Process Intensification, 2018. **129**: p. 28-36.
32. Wongchanapai, S., et al., *Performance evaluation of an integrated small-scale SOFC-biomass gasification power generation system.* Journal of Power Sources, 2012. **216**: p. 314-322.
33. Gholamian, E., V. Zare, and S.M. Mousavi, *Integration of biomass gasification with a solid oxide fuel cell in a combined cooling, heating and power system: A thermodynamic and environmental analysis.* International Journal of Hydrogen Energy, 2016. **41**(44): p. 20396-20406.
34. Doherty, W., A. Reynolds, and D. Kennedy, *Computer simulation of a biomass gasification-solid oxide fuel cell power system using Aspen Plus.* Energy, 2010. **35**(12): p. 4545-4555.
35. Yi, Y., et al., *Analysis and optimization of a solid oxide fuel cell and intercooled gas turbine (SOFC–ICGT) hybrid cycle.* Journal of Power Sources, 2004. **132**(1-2): p. 77-85.
36. Zhao, H., T. Jiang, and H. Hou, *Performance analysis of the SOFC–CCHP system based on H2O/Li–Br absorption refrigeration cycle fueled by coke oven gas.* Energy, 2015. **91**: p. 983-993.
37. Ishida, M., M. Yamamoto, and T. Ohba, *Experimental results of chemical-looping combustion with NiO/NiAl2O4 particle circulation at 1200 C.* Energy Conversion and Management, 2002. **43**(9-12): p. 1469-1478.
38. Tijani, M.M., E. Mostafavi, and N. Mahinpey, *Process simulation and thermodynamic analysis of a chemical looping combustion system using methane as fuel and NiO as the oxygen carrier in a moving-bed reactor.* Chemical Engineering and Processing - Process Intensification, 2019. **144**: p. 107636.
39. Fan, J., et al., *Thermodynamic evaluation of chemical looping combustion for combined cooling heating and power production driven by coal.* Energy Conversion and Management, 2017. **135**: p. 200-211.
40. Parvez, A., I.M. Mujtaba, and T. Wu, *Energy, exergy and environmental analyses of conventional, steam and CO2-enhanced rice straw gasification.* Energy, 2016. **94**: p. 579-588.
41. Zhu, L., P. Jiang, and J. Fan, *Comparison of carbon capture IGCC with chemical-looping combustion and with calcium-looping process driven by coal for power generation.* Chemical Engineering Research and Design, 2015. **104**: p. 110-124.

42. Dhanavath, K.N., et al., *Oxygen–Steam Gasification of Karanja Press Seed Cake: Fixed Bed Experiments, ASPEN Plus Process Model Development and Benchmarking with Saw Dust, Rice Husk and Sunflower Husk.* Journal of Environmental Chemical Engineering, 2018. **6**(2): p. 3061-3069.
43. Hannula, I. and E. Kurkela, *A parametric modelling study for pressurised steam/O2-blown fluidised-bed gasification of wood with catalytic reforming.* Biomass and bioenergy, 2012. **38**: p. 58-67.
44. Hannula, I. and E. Kurkela, *A semi-empirical model for pressurised air-blown fluidised-bed gasification of biomass.* Bioresource technology, 2010. **101**(12): p. 4608-4615.
45. Parvez, A.M., et al., *Bio-DME production based on conventional and CO 2-enhanced gasification of biomass: A comparative study on exergy and environmental impacts.* Biomass and Bioenergy, 2018. **110**: p. 105-113.
46. Al-Sulaiman, F.A., I. Dincer, and F. Hamdullahpur, *Exergy analysis of an integrated solid oxide fuel cell and organic Rankine cycle for cooling, heating and power production.* Journal of power sources, 2010. **195**(8): p. 2346-2354.
47. Zhang, X., et al., *Exergetic and exergoeconomic assessment of a novel CHP system integrating biomass partial gasification with ground source heat pump.* Energy Conversion and Management, 2018. **156**: p. 666-679.
48. Campanari, S., *Thermodynamic model and parametric analysis of a tubular SOFC module.* Journal of Power Sources, 2001. **92**(1-2): p. 26-34.
49. Linderholm, C., T. Mattisson, and A. Lyngfelt, *Long-term integrity testing of spray-dried particles in a 10-kW chemical-looping combustor using natural gas as fuel.* Fuel, 2009. **88**(11): p. 2083-2096.
50. Wolf, J., M. Anheden, and J. Yan, *Comparison of nickel-and iron-based oxygen carriers in chemical looping combustion for CO2 capture in power generation.* Fuel, 2005. **84**(7-8): p. 993-1006.
51. Minutillo, M., A. Perna, and D. Di Bona, *Modelling and performance analysis of an integrated plasma gasification combined cycle (IPGCC) power plant.* Energy Conversion and Management, 2009. **50**(11): p. 2837-2842.
52. Ding, G., et al., *Process simulation and optimization of municipal solid waste fired power plant with oxygen/carbon dioxide combustion for near zero carbon dioxide emission.* Energy Conversion and Management, 2018. **157**: p. 157-168.
53. Murphy, J.D. and E. McKeogh, *Technical, economic and environmental analysis of energy production from municipal solid waste.* Renewable energy, 2004. **29**(7): p. 1043-1057.
54. Perna, A., M. Minutillo, and E. Jannelli, *Hydrogen from intermittent renewable energy sources as gasification medium in integrated waste gasification combined cycle power plants: A performance comparison.* Energy, 2016. **94**: p. 457-465.